



HAL
open science

Electronic structure and magnetic properties of the effective spin $J_{\text{eff}} = 1/2$ two-dimensional triangular lattice $K_3\text{Yb}(\text{VO}_4)_2$

U. Voma, S. Bhattacharya, Edwin Kermarrec, J. Alam, Y. Jana, B. Sana, P. Khuntia, S. Panda, B. Koteswararao

► **To cite this version:**

U. Voma, S. Bhattacharya, Edwin Kermarrec, J. Alam, Y. Jana, et al.. Electronic structure and magnetic properties of the effective spin $J_{\text{eff}} = 1/2$ two-dimensional triangular lattice $K_3\text{Yb}(\text{VO}_4)_2$. *Physical Review B*, 2021, 104 (14), pp.144411. 10.1103/PhysRevB.104.144411 . hal-04312166

HAL Id: hal-04312166

<https://hal.science/hal-04312166>

Submitted on 28 Nov 2023

HAL is a multi-disciplinary open access archive for the deposit and dissemination of scientific research documents, whether they are published or not. The documents may come from teaching and research institutions in France or abroad, or from public or private research centers.

L'archive ouverte pluridisciplinaire **HAL**, est destinée au dépôt et à la diffusion de documents scientifiques de niveau recherche, publiés ou non, émanant des établissements d'enseignement et de recherche français ou étrangers, des laboratoires publics ou privés.

Electronic structure and magnetic properties of the effective spin $S = 1/2$ 2D triangular lattice $\text{K}_3\text{Yb}(\text{VO}_4)_2$

U. K. Voma,¹ S. Bhattacharya,² E. Kermarrec,² J. Alam,³ Y. M. Jana,³ B. Sana,⁴ P. Khuntia,⁴ S. K. Panda,^{5,*} and B. Koteswararao^{1,†}

¹*Department of Physics, Indian Institute of Technology Tirupati, Tirupati 517506, India*

²*Université Paris-Saclay, CNRS, Laboratoire de Physique des Solides, 91405, Orsay, France*

³*Department of Physics, University of Kalyani, Kalyani 741235, India*

⁴*Department of Physics, Indian Institute of Technology Madras, Chennai 600036, India*

⁵*Department of Physics, Bennett University, Greater Noida 201310, India*

(Dated: September 18, 2021)

Abstract

We report the structural, magnetic, specific heat, and electronic structure studies of the material $\text{K}_3\text{Yb}(\text{VO}_4)_2$, which has two-dimensional triangular layers constituted by rare-earth magnetic Yb^{3+} ions. Magnetic susceptibility data shows the absence of magnetic long-range order down to 0.5 K. No bifurcation is observed between zero-field-cooled and field-cooled magnetic susceptibility data ruling out the possibility of spin-glassiness down to 0.5 K. From the fit to magnetic susceptibility data with Curie-Weiss law in the low-temperature region, the observed Curie-Weiss temperature (θ_{CW}) is about -1 K, implying an antiferromagnetic coupling between the Yb^{3+} ions. Magnetic field-dependent specific heat fits well with two-level Schottky behavior. The analysis of magnetization and specific heat data confirms that the Yb^{3+} ion hosts the effective spin-1/2 state. To provide a microscopic understanding of the ground state nature of the titled material, we carried out state-of-the-art first-principle calculations based on density functional theory + Hubbard U (DFT+U) and density functional theory + dynamical mean-field theory (DFT+DMFT) approaches. Our calculations reveal that the system belongs to the novel class of spin-orbit driven Mott Hubbard insulators and possesses large in-plane magnetocrystalline anisotropy.

PACS numbers:

I. INTRODUCTION

Geometrically Frustrated Magnetism in two-dimensional (2D) magnetic materials draw significant attention to the scientific community due to their storming and unique magnetic properties. The strong quantum fluctuation enhanced by competing interaction between spins leads to unusual ground states. In $S = 1/2$ Heisenberg 2D triangular spin systems, the quantum fluctuations are more robust, which prevents the magnetic long-range order (LRO) even at $T = 0$ K in the presence of anisotropic exchange **interactions arises from spin-orbit coupling (SOC)**, and can exhibit the novel disordered ground state called Quantum Spin Liquid (QSL) as contemplated by P. W. Anderson [1]. The spins in the QSL state can be highly entangled with each other, even at long distances. The QSL state has been proposed experimentally for various 2D geometrically frustrated magnetic systems (GFMS), such as triangular and Kagome lattices, with gapped and gapless fractionalized spin excitations without a conventional symmetry breaking phase transition [2–4]. A few well-known $S = 1/2$ QSL materials in 2D GFMS are κ -(BEDT-TTF)₂Cu₂(CN)₃ [5, 6], EtMe₃Sb[Pd(mit)₂]₂ [7, 8], and ZnCu₃(OH)₆Cl₂ [9–11].

Recently, the interest in understanding the physics of $S = 1/2$ quantum magnetism is expanded from the 3d to

4d, 5d, and 4f rare-earth-based magnetic systems. The effective $S = 1/2$ can be realized in some of the Ru^{3+} , Ir^{4+} , Ce^{3+} , Yb^{3+} based materials due to the strong spin-orbit coupling and crystal electric field (CEF) effects, which lead to exotic quantum phenomena. A few exemplar materials of this class are 4d honeycomb lattice α - RuCl_3 [12], 5d honeycomb lattices A_2IrO_3 , (A=Li, Na, Cu) [13–15] and $\text{H}_3\text{LiIr}_2\text{O}_6$ [16], 4f- Yb^{3+} based triangular lattices YbMgGaO_4 [17–23], YbZnGaO_4 [24], and NaYbX_2 (X=O, S, Se), etc. [25–30].

In the compound YbMgGaO_4 , the magnetic, specific heat (C_p), Muon spin relaxation (μSR), and inelastic neutron scattering (INS) measurements revealed the absence of static magnetic LRO down to several mK temperatures, despite an antiferromagnetic coupling strength with the Curie-Weiss temperature (θ_{CW}) of -4 K. **The magnetic specific heat C_m data in the low-temperature region follow the power-law temperature dependence as $C_m \sim T^\alpha$. Furthermore, the value of α close to 2/3 suggests the possible realization of a gapless QSL state for the triangular Heisenberg antiferromagnetic lattice** [17]. Electron spin resonance (ESR) study revealed the anisotropic nature of the spin interactions [18]. The μSR relaxation rate exhibits a temperature-independent plateau behavior at low temperatures suggesting persistent spin dynamics [19]. The INS measurements revealed continuous diffusive magnetic excitations suggesting that YbMgGaO_4 might host a gapless QSL with a spinon Fermi surface [20, 22]. While the isotropic perfect $S = 1/2$ 2D triangular lattice model with nearest-neighbor (NN) interactions yield a 120° Néel state theo-

*Electronic address: swarup.panda@bennett.edu.in

†Electronic address: koteswararao@iittp.ac.in

retically at $T = 0$ K [32, 33], the origin of QSL state in the compound YbMgGaO_4 could be due to strong spin-orbit coupling (SOC) effects. From the recent arguments, in comparison with YbZnGaO_4 , it was also pointed that YbMgGaO_4 showed a spin glass-like ground state from the observations of frequency-dependent magnetic susceptibility [24], which was alternatively explained as a tiny spin freezing [23]. As the ground state of this system is still under debate due to the site mixing of Ga^{3+} and Mg^{2+} ions, the exploration of suitable candidate materials is required to understand the physics behind the 2D $S = 1/2$ triangular lattice whether the strong SOC or disorder-induced anisotropy drives the QSL state.

The study of rare-earth-based 2D triangular magnetic materials without site disorder has attracted attention in searching the novel QSL states. The series of rare-earth chalcogenides NaYbX_2 were identified as promising QSL candidates. In the case of NaYbO_2 , no magnetic LRO down to 50 mK is revealed. Furthermore, a field-induced quantum phase transition was observed above an applied field of 2 T [26]. On the other hand, the pressure-induced metallic states were observed in NaYbSe_2 [30], indicating that these rare-earth chalcogenides offer an ideal venue to discuss QSL nature and superconductivity as predicted by P. W. Anderson. To understand further interesting properties of 2D triangular GFMS, there is a necessity to discover promising materials of this category.

Herein, we introduce another structurally perfect triangular lattice system $\text{K}_3\text{Yb}(\text{VO}_4)_2$ [34], with the 2D triangular lattices of Yb^{3+} ions. Yb^{3+} hosts effective $S = 1/2$ moments as found below. Based on the measured magnetic and specific heat data, we find that the system does not exhibit any LRO down to 0.5 K. The obtained θ_{CW} of -1 K indicates weak antiferromagnetic coupling between the Yb^{3+} ions. This is further supported by the computed exchange interactions using the LSDA+U method. We analyzed the detailed electronic structure based on LSDA+U and LDA+DMFT methods and found that the insulating state in $\text{K}_3\text{Yb}(\text{VO}_4)_2$ arises due to the combined effects of SOC and electronic correlations. Our results indicate that this system possesses a large magnetic crystalline anisotropy. We also found that the dynamical correlation effects are crucial for accurately describing the f -multiplet spectra.

II. EXPERIMENTAL AND COMPUTATIONAL DETAILS:

We have synthesized the polycrystalline material $\text{K}_3\text{Yb}(\text{VO}_4)_2$ using the conventional solid-state synthesis method. Initially, the rare-earth oxide Yb_2O_3 was fired at 1000°C for 6 hours to remove the moisture and absorbed CO_2 . It was then mixed with K_2CO_3 , V_2O_5 in stoichiometric proportion and ground thoroughly. The pressed pellets are placed in an alumina crucible and fired at 750°C for 48 hours with several intermediate grindings. To confirm the single-phase, the X-ray diffraction

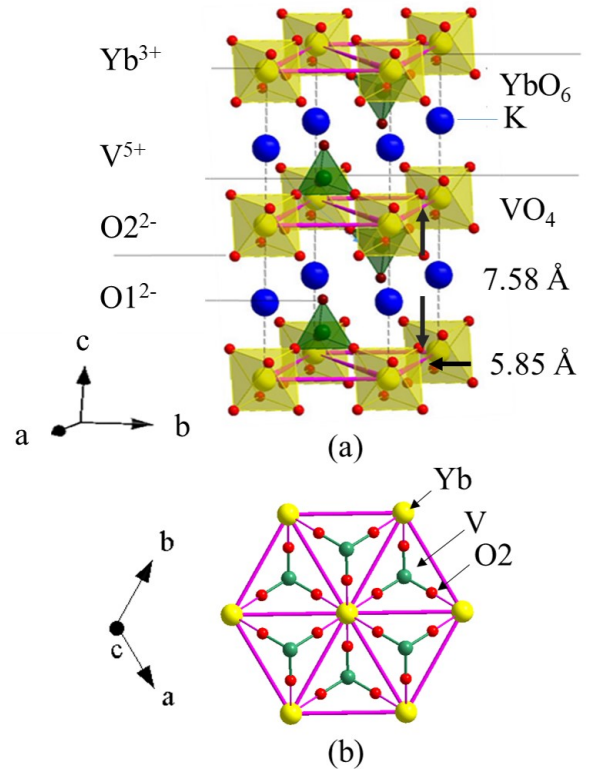


Figure 1: (color online). (a) Crystal structure built with the YbO_6 octahedra, VO_4 tetrahedra, and K atoms. (b) The 2D triangular lattices of Yb^{3+} ions. Yb^{3+} hosts effective $S = 1/2$ moments as found below. Based on the measured magnetic and specific heat data, we find that the system does not exhibit any LRO down to 0.5 K. The obtained θ_{CW} of -1 K indicates weak antiferromagnetic coupling between the Yb^{3+} ions. This is further supported by the computed exchange interactions using the LSDA+U method. We analyzed the detailed electronic structure based on LSDA+U and LDA+DMFT methods and found that the insulating state in $\text{K}_3\text{Yb}(\text{VO}_4)_2$ arises due to the combined effects of SOC and electronic correlations. Our results indicate that this system possesses a large magnetic crystalline anisotropy. We also found that the dynamical correlation effects are crucial for accurately describing the f -multiplet spectra.

Table I: The atomic coordinates for $\text{K}_3\text{Yb}(\text{VO}_4)_2$

Atom type	Wyckoff position	Site	x	y	z	Occupancy
Yb(1)	1b	-3m	1	0	0.5	1
K(1)	2d	3m	0.6667	0.3333	1.2961	1
K(2)	1a	-3m	0	0	1	1
V(1)	2d	3m	0.6667	0.3333	0.7474	1
O(1)	2d	3m	0.6667	0.3333	0.9595	1
O(2)	6i	m	0.3499	0.1750	0.6693	1

(XRD) measurements were carried out at room temperature. The temperature (T) and magnetic field (H) dependent magnetization (M) were done using Vibrating Sample Magnetometer (VSM) down to 5 K and superconducting quantum interference device (SQUID) magnetometer used to do the measurements down to 0.5 K, attached to Physical Property Measurement System (PPMS), Quantum Design, *Inc.* Specific heat as a function of temperature $C_p(T)$ measurements were performed in several applied magnetic fields using PPMS down to 2 K.

We have carried out both non-spin and spin-polarized electronic structure calculations using density functional

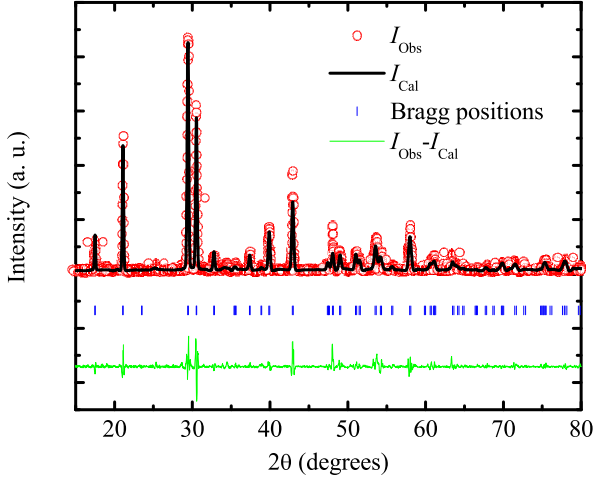


Figure 2: (color online). Refinement of the X-ray diffraction data measured at room temperature for $\text{K}_3\text{Yb}(\text{VO}_4)_2$ polycrystalline sample.

theory (DFT) [41, 42] with local density approximation (LDA) and local spin-density approximation+Hubbard U (LSDA+ U) [43] approaches as implemented in the all-electron, full potential code WIEN2K [44]. The Brillouin-Zone integration is performed with a $12 \times 12 \times 8$ k -mesh. To achieve energy convergence of the eigenvalues, the wave functions in the interstitial region were expanded in plane waves with a cutoff $R_{MT}k_{max} = 8$, where R_{MT} denotes the smallest atomic sphere radius and k_{max} represents the magnitude of the largest k vector in the plane wave expansion. The valence wave functions inside the spheres are expanded up to $l_{max} = 10$, while the charge density is Fourier expanded up to a large value of $G_{max} = 12$. Based on the converged non-spin polarized LDA solutions, we constructed the maximally localized Wannier function for the f like bands, using the Wien2wannier [45] and WANNIER90 codes [46] to compute the hopping parameters between the effective Yb- f orbitals.

We also carried out LSDA+ U calculations using the full potential linearized augmented plane wave method (FP-LAPW) as implemented in the RSPt code [47, 48]. The consistency of the results from RSPt and Wien2k provides further credence to our calculations. Using the LSDA+ U solutions of RSPt, we employed the magnetic force theorem [50, 51] to extract the effective inter-site exchange parameters (J_{ij}). A detailed discussion of the implementation of the magnetic force theorem in RSPt is provided in Ref. [52]. The J_{ij} are extracted in a linear-response manner via Green's function technique.

Considering that the many-body effects are extremely significant for the highly correlated f -states, we also performed LDA+DMFT simulations using the same RSPt code [48]. In this implementation [52–56] of

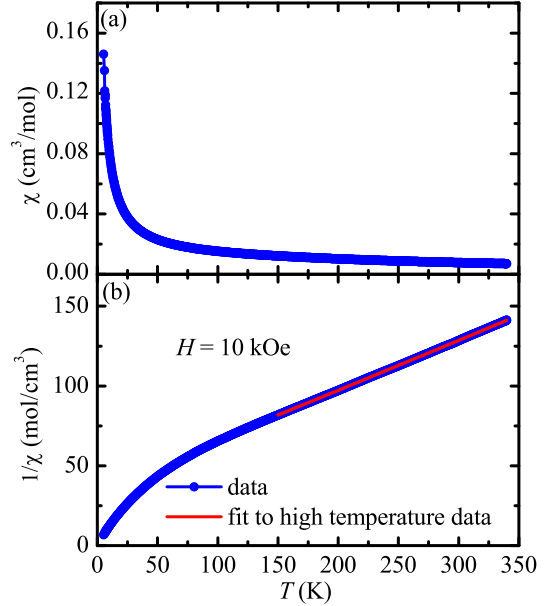


Figure 3: (color online). (a) The magnetic susceptibility $\chi(T)$ of $\text{K}_3\text{Yb}(\text{VO}_4)_2$ at the applied magnetic field 10 kOe, (b) The inverse-magnetic susceptibility data with the fit to the expression $1/[\chi_0 + C_{HT}/(T - \theta_{HT})]$.

LDA+DMFT, the many-body corrections appear in a form that depends on a self-consistently calculated density matrix and on the correlated orbitals, which are $4f$ states on the Yb atoms in the present case. The effective impurity problem in the LDA+DMFT calculations has been solved through the Hubbard I (HIA) solver. The reported results are based on a single-shot simulation where the convergence of the self-energy has been achieved with 5000 Matsubara frequencies, and the temperature is taken as 150 K.

To describe the electronic correlation effect within LSDA+ U and LDA+DMFT approaches, we have taken $U = 4.0$ eV, $J = 0.5$ eV for Yb- f states which are obtained from a constrained random phase approximation (cRPA) calculations [57] using the implementation of Ref. [58]. This method has been successfully used for several transition metal oxides. The first-principle estimation of U using cRPA ensures that the reported electronic and magnetic properties are completely parameter-free and thus, our approach is truly *ab-initio*.

III. STRUCTURAL DETAILS:

The structure of $\text{K}_3\text{Yb}(\text{VO}_4)_2$ belongs to the family of Glaserite, having the general formula $\text{A}_3\text{RE}(\text{VO}_4)_2$ (A - alkali metal, RE - rare-earth) with trigonal crys-

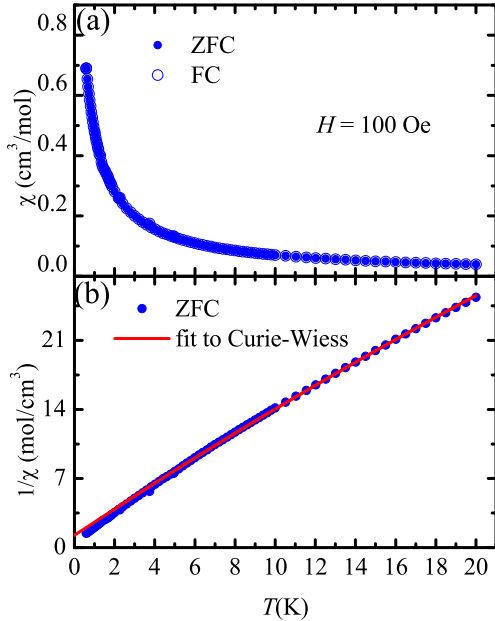


Figure 4: (color online). (a) Temperature-dependent ZFC and FC $\chi(T)$ plot in the range from 0.5 K to 20 K. (b) Inverse- χ versus T plot with the Curie-Weiss fit (represented by solid line).

tal system of $P\bar{3}m1$ (No. 164) space group [34]. **The measured x-ray diffraction data is used for the refinement using Fullprof software [40] as shown in the Fig. 2. The refinement parameters are $R_p = 12.5, R_{wp} = 17.1$, and $\chi^2 = 2$. The extracted lattice parameters $a = b = 5.85 \text{ \AA}$, $c = 7.58 \text{ \AA}$, $\alpha = \beta = 90^\circ$, $\gamma = 120^\circ$ are well consistent with Ref. [34]. The position coordinates and occupancies of different atoms in the crystal structure are mentioned in the table I. The crystal structure is constituted with VO_4 tetrahedra, YbO_6 octahedra, and K atoms. Fig. 1(a) shows the crystal structure of the $\text{K}_3\text{Yb}(\text{VO}_4)_2$ in which Yb atoms are placed in a well-separated 2D triangular lattice with NN distance 5.85 \AA . The inter-layer separation 7.58 \AA is larger than the intra-layer distance of Yb-Yb. **The ratio between the inter-layer and intra-layer distance (d_{inter}/d_{intra}) is only 1.29. This ratio for the $\text{K}_3\text{Yb}(\text{VO}_4)_2$ compound is smaller than the values of 1.7 for NaYbO_2 and 2.4 for YbMgGaO_4 . However, it is somewhat similar to those of other 2D triangular layered materials with the ratio of $d_{inter}/d_{intra} \sim 1.1$ for $\text{NaBaYb}(\text{BO}_3)_2$ and $d_{inter}/d_{intra} \sim 1.43$ for $\text{Rb}_3\text{Yb}(\text{PO}_4)_2$, which show the magnetic frustration and QSL features [35, 36].****

The bond-length of Yb-O2 in YbO_6 octahedra is 2.19 \AA . The environment of Yb^{3+} holds D_{3d} point

group symmetry, and less distorted in comparison to NaYbO_2 , YbMgGaO_4 . The presence of the inversion center between the bonds that precludes antisymmetric Dzyaloshinskii–Moriya (DM) exchange interactions. The 2D triangular layers are separated by K atomic layers. The possible magnetic exchange path, in the titled compound is through Yb-O2-V-O2-Yb while it is through only O atoms in NaYbO_2 and YbMgGaO_4 [17, 26]. In this path the bond angles are $\text{Yb-O2-V} \approx 164.4^\circ$, $\text{O2-V-O2} \approx 108.7^\circ$

IV. RESULTS:

A. Magnetic properties:

Temperature-dependent magnetization measurements were performed in the presence of a magnetic field 10 kOe. The magnetic susceptibility χ and inverse-magnetic susceptibility χ^{-1} as a function of temperature (T) down to 5 K is shown in Fig. 3. The χ^{-1} data are fitted with the expression $(T - \theta_{HT})/C_{HT}$ on a high-temperature region from 150 K to 340 K (see Fig. 3(b)). The value of Curie constant at high temperature (C_{HT}) is obtained to be $3.2 \text{ cm}^3\text{K/mol}$, which gives $J = 7/2$ and $g_J = 1.28$. The obtained value of g_J is close to the expected value $g_J = 8/7 \approx 1.14$. The high-temperature Curie-Weiss temperature is found to be $\theta_{HT} \approx -110 \text{ K}$. The large value of θ_{HT} is not due to the magnetic exchange couplings, but it results from the CEF effect on the Yb atom. As the total angular momentum $J = 7/2$ (holds eight-fold degeneracy) is in the CEF environment of D_{3d} symmetry, the energy levels split into four Kramers doublets by preserving the time-reversal symmetry. The energy difference between the ground state doublet and the first excited state of Kramers doublet, is defined as the CEF gap (Δ_{CEF}). We have tabulated II the Δ_{CEF} values for a few of Yb^{3+} based triangular materials along with the high-temperature values of θ_{HT} (see table II). As the value of θ_{HT} of $\text{K}_3\text{Yb}(\text{VO}_4)_2$ is close to the value of NaYbO_2 compound, the Δ_{CEF} of $\text{K}_3\text{Yb}(\text{VO}_4)_2$ could also be similar to that of NaYbO_2 (404 K) [25]. While the Δ_{CEF} is expected to be large (as we found θ_{HT} is about -110 K), the spin tends to lie in the ground state and hosts the effective spin-1/2 ($S_{eff} = 1/2$) at the low-temperature region.

The zero field cooled (ZFC) and field cooled (FC) susceptibility with temperature variation down to 0.5 K is shown in Fig. 4(a). No bifurcation is noticed, which represents the absence of spin freezing or spin glass transition. As shown in Fig. 4(b), the fit to the formula $1/[\chi_0 + C_{LT}/(T - \theta_{LT})]$ in the temperature range 1.8 – 20 K gives $\theta_{LT} \approx -1 \text{ K}$. The temperature-independent susceptibility is found to be $\chi_0 \approx 4.6 \times 10^{-3} \text{ cm}^3/\text{mol}$. After subtracting the core diamagnetic susceptibility $\chi_{dia} \approx -1.61 \times 10^{-4} \text{ cm}^3/\text{mol}$ calculated from the individual ions values [59], the obtained Van-Vleck susceptibility is $\chi_{VV} \approx 4.76 \times 10^{-3} \text{ cm}^3/\text{mol}$. The Curie con-

Table II: The crystal electric field gaps (Δ_{CEF}) of various Yb-based compounds

2D triangular lattice	YbO ₆ Environment	θ_{HT} (K)	Δ_{CEF} (K)
NaYbS ₂	D _{3d}	-65	197 [28]
NaYbSe ₂	D _{3d}	-60	183 [31]
NaYbO ₂	D _{3d}	-100	404 [25]
K ₃ Yb(VO ₄) ₂	D _{3d}	-110	to be measured

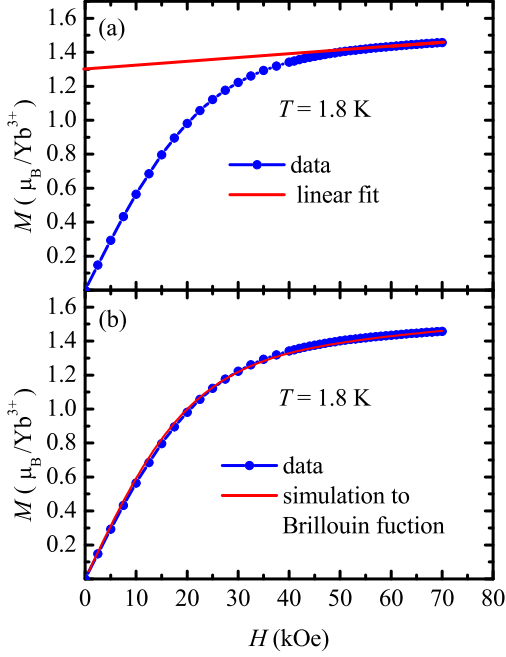


Figure 5: (color online). (a) Magnetic field-dependent magnetization at $T = 1.8$ K. The solid straight line represents the extrapolation to linear fit in the range 60 – 70 kOe. (b) The data with simulation to Brillouin function for $S = 1/2$ and $g \approx 2.6$.

stant C_{LT} provides the magnetic moment $\mu_{\text{eff}} \approx 2.41 \mu_{\text{B}}$. As compared to the value $\mu_{\text{eff}} \approx 4.53 \mu_{\text{B}}$ for free ions, the reduced value of the magnetic moment in the low-temperature region is due to the presence of $S = 1/2$ doublet as the ground state of Yb³⁺ ion with the effective spin $S_{\text{eff}} = 1/2$ with $g \approx 2.75$. The nonlinear variation of the field-dependent magnetization plot at 1.8 K is shown in Fig. 5. The saturation magnetic moment is about $1.3 \mu_{\text{B}}/\text{Yb}^{3+}$ obtained from the intercept of the linear fit as shown in Fig. 5(a). The Fig. 5(b) displays the $M(H)$ data matches with the simulation to the Brillouin function for $S_{\text{eff}} = 1/2$, $g \approx 2.6$ at $T = 1.8$ K ($> \theta_{\text{LT}}$).

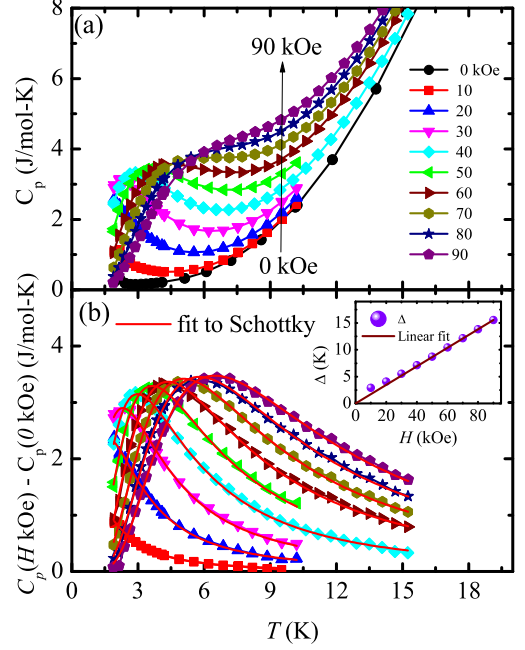


Figure 6: (color online). (a) Temperature-dependent specific heat C_p at different applied magnetic fields from 0 kOe to 90 kOe. (b) The specific heat after subtracting the zero field data with the fit to Schottky anomaly (see the text). The two energy level Schottky fit after subtracting the specific heat at 0 T. The inset shows the energy gap variation with applied magnetic fields.

B. Specific heat measurements:

The specific heat data as a function of temperature ($C_p(T)$) were measured down to 1.8 K in different magnetic fields upto 90 kOe. As shown in Fig. 6(a), we did not observe any sharp transition in zero-field data. Field-dependent behavior is observed. A broad peak is seen in the presence of magnetic fields. The broad peak moves towards high temperatures with increasing magnetic fields due to the Zeeman splitting of the ground state Kramers doublet ($S_{\text{eff}} = \pm 1/2$). The two-level Schottky fit $C = Nk_{\text{B}} \frac{(\Delta/T)^2 e^{-\Delta/T}}{(1+e^{-\Delta/T})^2}$ to the $C_p(H \text{ kOe}) - C_p(0 \text{ kOe})$

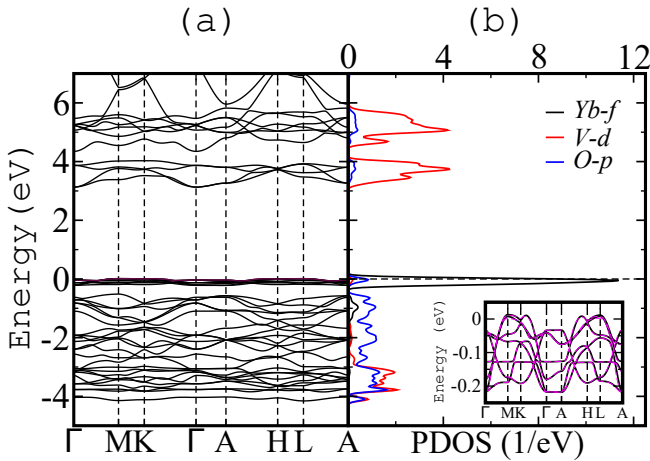


Figure 7: (color online). Non-spin-polarized LDA. (a) Band dispersion along various high symmetry directions, and (b) orbital projected partial density of states of Yb- f , V- d , and O- p states. For clarity, the f states are plotted after scaling the PDOS by a factor of 0.2. Inset of (b) shows the Wannier-interpolated bands superimposed on the LDA bands, plotted in the narrow energy region around the Fermi level.

Table III: Hopping integrals t (in meV) between the NN Yb- f states.

	Yb- fxz^2	Yb- fyz^2
Yb- fxz^2	-1.5	-0.38
Yb- fyz^2	-0.38	-1.5

$C_p(0 \text{ kOe})$ data is shown in Fig. 6(b). The extracted Zeeman energy gap (Δ) between the energy levels of the ground state doublet $S_{\text{eff}} = \pm 1/2$ increases linearly with the applied magnetic fields. The g value yielded from the slope of the linear fit to the expression $\Delta = g\mu_B H$ is about 2.5, in good agreement with the value estimated from the magnetic measurements.

C. Basic Electronic Structure:

To begin with, we have analyzed the band structure and partial density of states (PDOS), obtained using the LDA method. The results of our calculations are presented in Fig. 7. Close to the Fermi level, we find seven almost dispersion less bands which give rise to the sharp peak observed in the PDOS of Yb- f (Fig. 7(b)), implying the strongly localized nature of the f states. These states are also mostly occupied and thus consistent with the nominal $3+$ (f^{13}) charge state of Yb-ions. The occupied O- p states appear in the energy range between -4 eV to -0.5 eV , while the V- d states are fully unoccupied, located above 3 eV from the Yb- f states. The hybridization between Yb- f and O- p states looks very weak.

Since the Yb- f states are well separated from the rest

Table IV: Energies of different magnetization axis with respect to the energy of c -axis magnetization (Δ_E). The corresponding spin moments μ_s , orbital moments μ_o , and total moments μ_{tot} ($\mu_s + \mu_o$) are tabulated.

	010 axis	110 axis	001 axis
Δ_E (meV/cell)	-98.4	-98.4	0.00
μ_s (μ_B/Yb)	0.80	0.80	0.95
μ_o (μ_B/Yb)	1.93	1.93	1.89
μ_{tot} (μ_B/Yb)	2.73	2.73	2.84

of the bands, and they only contribute to the Fermi surface, we constructed the effective Wannier functions for these bands using the WANNIER90 formalism [46] where only the Yb- f states were kept in the basis, and the rest of the orbitals were downfolded. In these calculations, we primarily find out the relevant orbitals for the magnetism and estimate the inter-site hopping strengths between them. The Wannier interpolated bands along with the LDA bands are shown in the inset of Fig.7(b), and the agreement is quite remarkable. The diagonalization of the obtained onsite blocks of the Yb- f Hamiltonian, gives the eigen-energies $-147, -128, -80, -80, -80, -56, -56 \text{ meV}$, corresponding to the eigen-states having predominant $fy(3x^2 - y^2), fz^3, fxyz, fz(x^2 - y^2), fx(x^2 - 3y^2), fxz^2, fyz^2$ characters, respectively. Since Yb is in f^{13} state, the above onsite energies indicate that all the lower-lying states ($fy(3x^2 - y^2), fz^3, fxyz, fz(x^2 - y^2), fx(x^2 - 3y^2)$) are completely filled up and thus magnetically inactive. However, the topmost degenerate states which have predominant fxz^2, fyz^2 character, are partially filled up and would contribute to the local moment formation. The computed inter-site hopping integrals between these two relevant orbitals is reported in table III. Interestingly, the magnitudes of the hopping parameters come out to be very weak. This also implies that the magnetic exchange interactions (J_{ij}) between the Yb-ions would be small. The estimation of the (J_{ij}) is discussed in the later part of the manuscript.

D. LSDA+U analysis of magnetic properties :

Next, in order to provide a microscopic understanding of the experimentally observed magnetization, we estimated the different terms necessary for constructing the spin Hamiltonian for this system. Apart from the external magnetic field-dependent Zeeman term, spin dynamics of a system are governed by the isotropic Heisenberg exchange, anisotropic Dzyaloshinskii-Moriya (DM) interaction, and the single-ion anisotropy or the magnetocrystalline anisotropy of the system. Using the formalism of Ref. [52], the estimated Yb-Yb magnetic-exchange interactions (J_{ij}) come out to be 0.1 meV and antiferromagnetic in nature. This is consistent with the low-temperature value of Curie-Weiss temperature (θ_{LT}) obtained from the fitting of experimental susceptibility. We

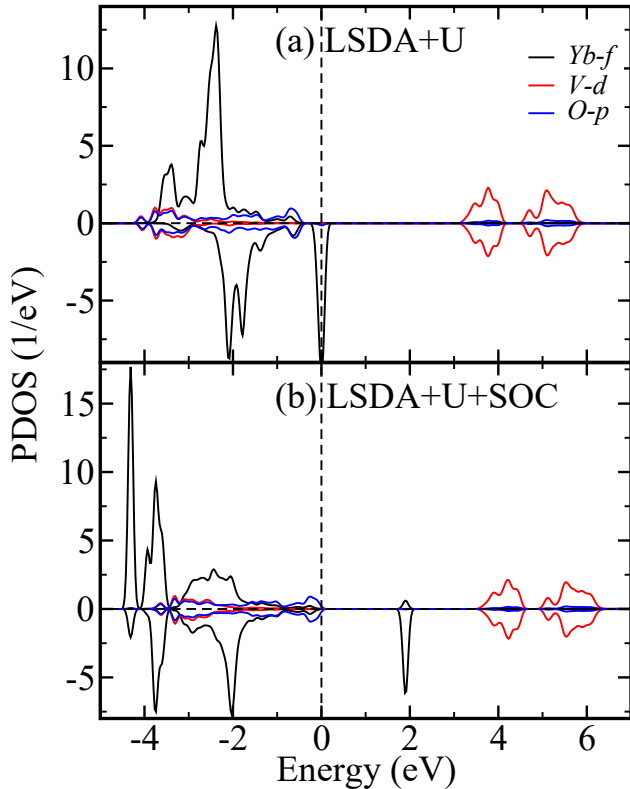


Figure 8: (color online). The partial density of states of Yb- f , V- d , and O- p in the spin polarized ground state obtained from LSDA+U and LSDA+U+SOC calculations.

note that such small antiferromagnetic exchange in the triangular Yb network might promote magnetic frustration at a very low temperature which will oppose long range ordering. The experimental magnetic data also shows that the system does not have LRO down to 0.5 K. Although the Yb- f electrons possess large SOC, but the presence of inversion symmetry in this system makes DM interactions to be zero.

To determine the magneto-crystalline anisotropy, we have computed total energies by fixing the spin axis along various possible directions within the LSDA+U approach incorporating SOC. The computed energies, spin, and orbital moments are displayed in Table IV. Our calculations suggest that the Yb spins favor ab -plane as the preferred plane of magnetization. We also find that the spin moment for the prefer spin-axis of the Yb $^{3+}$ ion is $0.80 \mu_B$, and the orbital moment is almost 2.4 times that of the spin moment, making the total moment ($2.73 \mu_B$). Another key finding of our LSDA+U+SOC calculations is that the system possesses a large easy plane magneto-crystalline anisotropy energy (MAE). As displayed in Table IV, the ab -plane is energetically favorable with the energy -98.4 meV.

The partial density of states of the Yb- f , V- d , and O- p states for both the spin channels obtained using

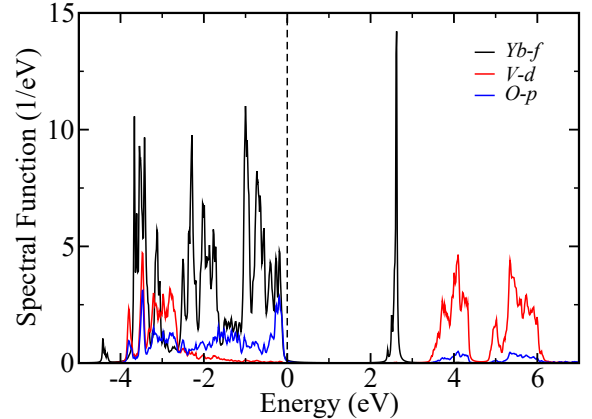


Figure 9: (color online). The partial density of states of Yb- f , V- d , and O- p in the paramagnetic state, obtained from LDA+DMFT+SOC simulations.

LSDA+U with, and without SOC has been shown in Fig. 8. We clearly see that SOC is crucial to open up the insulating gap in this system. Our results show that the majority Yb- f states are completely occupied, and located between -4.5 eV to -1.8 eV, and the gap opens up in the minority channel. This is expected since Yb is in a nominal $3+$ charge state (f^{13}), the first 7 electrons occupy the majority channel, while the rest 6 electrons fill up the minority f states, keeping only one level empty. The value of the insulating gap comes out to be 1.9 eV which is a p - f gap as the p states appear just below the Fermi level. Therefore according to the LSDA+U theory, this system is a charge-transfer insulator which is an unlikely electronic state for f -electron systems. However, it is well known that LSDA+U has limited success in describing the electronic structure of f -electron systems. Moreover, LSDA+U method works with symmetry broken solutions, and thus appropriate description of the paramagnetic electronic structure is outside its capabilities, necessitating the need of investigation using methods that are beyond the static mean-field approach.

E. Electronic structure from LDA+DMFT:

In view of the fact that an accurate treatment of the many-body electronic correlation is crucial for describing the correlated paramagnetic state of $K_3Yb(VO_4)_2$, we have employed LDA+DMFT with HIA incorporating SOC. In Fig. 9, we report the spectral function obtained in LDA+DMFT, which for simplicity, we will also label as PDOS. The obtained band-gap 2.2 eV, which is slightly larger than that of LSDA+U. Most importantly, contrary to the LSDA+U results, the gap is observed between the f -states, and the origin of this gap is a combined effect of SOC, and electron-electron correlation. Thus we can

conclude that $\text{K}_3\text{Yb}(\text{VO}_4)_2$ belongs to the very interesting class of spin-orbit driven Mott-Hubbard insulators. We note here that our LDA+DMFT calculations not only find out the correct nature of the insulating ground state but also provide the correct position of the f -multiplets.

V. DISCUSSION AND CONCLUSION

The ideal 2D Heisenberg triangular lattice hosts 120° Néel ordered state at absolute temperature $T = 0$ K [32, 33]. In the presence of 3D couplings, the system will order at finite temperature. For example, the 2D triangular lattice materials $\text{Ba}_3\text{CoSb}_2\text{O}_9$ [37], and $\text{Ba}_3\text{CoNb}_2\text{O}_9$ [38] shows magnetic LRO below the temperatures 3.7 K, and 1.4 K, respectively. Recently there have been extensive theoretical studies on the effect of strong SOC coupling on a triangular lattice. As per the spin-orbit coupled triangle lattice model, the possibility of various QSL phases was discussed. QSL state would be achieved due to strong SOC, which mainly generates highly anisotropic interactions. In the reference [39], the detailed study was carried on the ground state phase diagram, the effects on spinon Fermi surface of the QSL in the presence of SOC, and due to the presence of 2^{nd} NN & 3^{rd} NN couplings. The 2^{nd} NN interactions create a Dirac QSL as the lowest energy state. The inclusion of even a very small 3^{rd} NN interaction can greatly stabilize the QSL phase. In

this line of theoretical studies, it is essential to synthesize, and investigate 2D triangular quantum spin materials with possibly the large SOC. Our title material is another type of material in addition to those of previously published materials YbMgGaO_4 , and AYbX_2 . The theoretical band structure calculations also confirmed that this material has large SOC, and in-plane anisotropy.

In conclusion, we have synthesized, and studied the magnetic properties, and performed the electronic structure calculations on a compound $\text{K}_3\text{Yb}(\text{VO}_4)_2$ having 2D triangular-lattice of Yb^{3+} ions. Our results confirm that Yb^{3+} holds $S_{\text{eff}} = 1/2$ moments with an antiferromagnetic coupling with θ_{CW} about -1 K. No magnetic LRO was found down to 0.5 K. Electronic structure calculations confirm that the system is a Mott insulator with large SOC, and sizeable magneto-crystalline anisotropy energy. Further low-temperature experiments, such as μSR , and INS, would be required to fully explore the nature of its ground state.

VI. ACKNOWLEDGMENT

B. K. thanks DST INSPIRE faculty award scheme, and NFIG grant from IIT Tirupati. E. K. acknowledges financial support from the labex PALM for the QuantumPyroMan project (ANR10-LABX-0039-PALM)

-
- [1] P. W. Anderson, Resonating valence bonds: a new kind of insulator?, *Mater. Res. Bull.* **8**,153 (1973).
 - [2] L. Balents, Spin liquids in frustrated magnets, *Nature (London)* **464**, 199 (2010).
 - [3] Y. Li, P. Gegenwart and A. A. Tsirlin, Spin liquids in geometrically perfect triangular antiferromagnets, *J. Phys.: Condens. Matter* **32**(22), 224004 (2020).
 - [4] C. Broholm, R. J. Cava, S. A. Kivelson, D. G. Nocera, M. R. Norman, T. Senthil, Quantum spin liquids, *Science* **367**, 0668 (2020).
 - [5] Y. Shimizu, K. Miyagawa, K. Kanoda, M. Maesato, G. Saito, Spin liquid state in an organic Mott insulator with a triangular lattice, *Phys. Rev. Lett.* **91**, 107001 (2003).
 - [6] T. Isono, T. Terashima, K. Miyagawa, K. Kanoda, and S. Uji, Quantum criticality in an organic spin-liquid insulator κ -(BEDT-TTF) $_2\text{Cu}_2(\text{CN})_3$, *Nat. Commun.* **7**, 13494 (2016).
 - [7] S. Yamashita, Y. Nakazawa, M. Oguni, Y. Oshima, H. Nojiri, Y. Shimizu, K. Miyagawa, K. Kanoda, Thermodynamic properties of a spin-1/2 spin-liquid state in a κ -type organic salt, *Nat. Phys.* **4**, 459 (2008).
 - [8] S. Yamashita, T. Yamamoto, Y. Nakazawa, M. Tamura, R. Kato, Gapless spin liquid of an organic triangular compound evidenced by thermodynamic measurements, *Nat. Commun.* **2**, 275 (2011).
 - [9] T. H. Han, J. S. Helton, S. Y. Chu, D. G. Nocera, J. A. Rodriguez-Rivera, C. Broholm, and Y. S. Lee, Fractionalized excitations in the spin-liquid state of a kagome-lattice antiferromagnet, *Nature* **492**, 406 (2012).
 - [10] J. S. Helton, K. Matan, M. P. Shores, E. A. Nytko, B. M. Bartlett, Y. Yoshida, Y. Takano, A. Suslov, Y. Qiu, J.-H. Chung, D. G. Nocera, and Y. S. Lee, Spin Dynamics of the Spin-1/2 Kagome Lattice Antiferromagnet $\text{ZnCu}_3(\text{OH})_6\text{Cl}_2$, *Phys. Rev. Lett.* **98**, 107204 (2007).
 - [11] P. Khuntia, M. Velazquez, Q. Barthélemy, F. Bert, E. Kermarrec, A. Legros, B. Bernu, L. Messio, A. Zorko, and P. Mendels, Gapless ground state in the archetypal quantum kagome antiferromagnet $\text{ZnCu}_3(\text{OH})_6\text{Cl}_2$, *Nat. Phys.* **16**, 469 (2020).
 - [12] A. Banerjee, J. Q. Yan, J. Knolle, C. A. Bridges, M. B. Stone, M. D. Lumsden, D. G. Mandrus, D. A. Tennant, R. Moessner, and S. E. Nagler, Neutron scattering in the proximate quantum spin liquid α - RuCl_3 , *Science* **356**, 1055 (2017).
 - [13] Y. Singh and P. Gegenwart, Antiferromagnetic Mott Insulating State in Single Crystals of the Honeycomb Lattice Material Na_2IrO_3 , *Phys. Rev. B* **82**, 064412 (2010).
 - [14] Y. S. Choi, C. H. Lee, S. Lee, S. Yoon, W. J. Lee, J. Park, A. Ali, Y. Singh, J. C. Orain, G. Kim, J. S. Rhyee, W. T. Chen, F. Chou, and K. Y. Choi, Exotic Low-Energy Excitations Emergent in the Random Kitaev Magnet Cu_2IrO_3 , *Phys. Rev. Lett.* **122**, 167202 (2019).
 - [15] K. Mehlawat, A. Thamizhavel, and Y. Singh, Heat capacity evidence for proximity to the Kitaev quantum spin liquid in A_2IrO_3 ($\text{A} = \text{Na}, \text{Li}$), *Phys. Rev. B* **95**, 144406 (2017).
 - [16] K. Kitagawa, T. Takayama, Y. Matsumoto, A. Kato, R. Takano, Y. Kishimoto, S. Bette, R. Dinnebier, G. Jackeli,

- and H. Takagi, A spin-orbital-entangled quantum liquid on a honeycomb lattice, *Nature* **554**, 341 (2018).
- [17] Y. Li, H. Liao, Z. Zhang, S. Li, F. Jin, L. Ling, L. Zhang, Y. Zou, L. Pi, Z. Yang, J. Wang, Z. Wu, Q. Zhang, Gapless quantum spin liquid ground state in the two-dimensional spin-1/2 triangular antiferromagnet YbMgGaO_4 , *Sci. Rep.* **5**, 16419 (2015).
- [18] Y. Li, G. Chen, W. Tong, L. Pi, J. Liu, Z. Yang, X. Wang, and Q. Zhang, Rare-Earth Triangular Lattice Spin Liquid: A Single-Crystal Study of YbMgGaO_4 , *Phys. Rev. Lett.* **115**, 167203 (2015).
- [19] Y. Li, D. Adroja, P. K. Biswas, P. J. Baker, Q. Zhang, J. J. Liu, A. A. Tsirlin, P. Gegenwart, and Q. M. Zhang, Muon Spin Relaxation Evidence for the U(1) Quantum SpinLiquid Ground State in the Triangular Antiferromagnet YbMgGaO_4 , *Phys. Rev. Lett.* **117**, 097201 (2016).
- [20] J. A. M. Paddison, M. Daum, Z. Dun, G. Ehlers, Y. Liu, M. B. Stone, H. Zhou, M. Mourigal, Continuous excitations of the triangular-lattice quantum spin liquid YbMgGaO_4 , *Nat. Phys.* **13**, 117 (2017).
- [21] Y. Li, D. Adroja, R. I. Bewley, D. Voneshen, A. A. Tsirlin, P. Gegenwart, and Q. Zhang, Crystalline Electric-Field Randomness in the Triangular Lattice Spin-Liquid YbMgGaO_4 , *Phys. Rev. Lett.* **118**, 107202 (2017).
- [22] Y. Shen, Y. D. Li, H. C. Walker, P. Steffens, M. Boehm, X. Zhang, S. Shen, H. Wo, G. Chen, J. Zhao, Fractionalized excitations in the partially magnetized spin liquid candidate YbMgGaO_4 , *Nat. Commun.* **9**, 4138 (2018).
- [23] Y. Li, S. Bachus, B. Liu, I. Radelytskyi, A. Bertin, A. Schneidewind, Y. Tokiwa, A. A. Tsirlin, and P. Gegenwart, Rearrangement of uncorrelated valence bonds evidenced by low-energy spin excitations in YbMgGaO_4 , *Phys. Rev. Lett.* **122**, 137201 (2019).
- [24] Z. Ma, J. Wang, Z. Y. Dong, J. Zhang, S. Li, S. H. Zheng, Y. Yu, W. Wang, L. Che, K. Ran, S. Bao, Z. Cai, P. Cermak, A. Schneidewind, S. Yano, J. S. Gardner, X. Lu, S. L. Yu, J. M. Liu, S. Li, J. X. Li, J. Wen, Spin-Glass Ground State in a Triangular-Lattice Compound YbZnGaO_4 , *Phys. Rev. Lett.* **120**, 087201 (2018).
- [25] L. Ding, P. Manuel, S. Bachus, F. Gruler, P. Gegenwart, J. Singleton, R. D. Johnson, H. C. Walker, D. T. Adroja, A. D. Hillier and A. A. Tsirlin, Gapless spin-liquid state in the structurally disorder-free triangular antiferromagnet NaYbO_2 , *Phys. Rev. B* **100**, 144432 (2019).
- [26] K. M. Ranjith, D. Dmytriieva, S. Khim, J. Sichelschmidt, S. Luther, D. Ehlers, H. Yasuoka, J. Wosnitza, A. A. Tsirlin, H. Kühne, and M. Baenitz, Field-induced instability of the quantum spin liquid ground state in the $J_{eff} = 1/2$ triangular-lattice compound NaYbO_2 , *Phys. Rev. B* **99**, 180401(R) (2019).
- [27] M. M. Bordelon, E. Kenney, C. Liu, T. Hogan, L. Posthuma, M. Kavand, Y. Lyu, M. Sherwin, N. P. Butch, C. Brown, M. J. Graf, L. Balents, and S. D. Wilson, Field-tunable quantum disordered ground state in the triangular-lattice antiferromagnet NaYbO_2 , *Nat. Phys.* **15**, 1058 (2019).
- [28] R. Sarkar, Ph. Schlender, V. Grinenko, E. Haeussler, Peter J. Baker, Th. Doert, and H.-H. Klauss, Quantum spin liquid ground state in the disorder free triangular lattice NaYbS_2 , *Phys. Rev. B* **100**, 241116(R) (2019).
- [29] P. L. Dai, G. Zhang, Y. Xie, C. Duan, Y. Gao, Z. Zhu, E. Feng, C. L. Huang, H. Cao, A. Podlesnyak, G. E. Granroth, and D. Voneshen, Spinon fermi surface spin liquid in a triangular lattice antiferromagnet NaYbSe_2 , arXiv:2004.06867 (2020).
- [30] Z. Zhang, Y. Yin, X. Ma, W. Liu, J. Li, F. Jin, J. Ji, Y. Wang, X. Wang, X. Yu, Q. Zhang, Pressure induced metallization and possible unconventional superconductivity in spin liquid NaYbSe_2 , arXiv:2003.11479 (2020).
- [31]) Z. Zhang, X. Ma, J. Li, G. Wang, D. T. Adroja, T. G. Perring, W. Liu, F. Jin, J. Ji, Y. Wang, X. Wang, J. Ma, and Q. Zhang, Crystalline Electric-Field Excitations in Quantum Spin Liquids Candidate NaYbSe_2 , arXiv:2002.04772(2020).
- [32] L. Capriotti, A. E. Trumper, and S. Sorella, Long-Range Néel Order in the Triangular Heisenberg Model, *Phys. Rev. Lett.* **82**, 3899 (1999).
- [33] S. R. White and A. L. Chernyshev, Néel Order in Square and Triangular Lattice Heisenberg Models, *Phys. Rev. Lett.* **99**, 127004 (2007).
- [34] M. M. Kimani, L. Thompson, W. Snider, C. D. McMillen and J. W. Kolis, Hydrothermal Synthesis and Spectroscopic Properties of a New Glaserite Material, $\text{K}_3\text{RE}(\text{VO}_4)_2$ (RE = Sc, Y, Dy, Ho, Er, Yb, Lu, or Tm) with Potential Lasing and Optical Properties, *Inorg. Chem.* **51**, 13271 (2012).
- [35] S. Guo, A. Ghasemi, C. L. Broholm, and R. J. Cava, Magnetism on ideal triangular lattices in $\text{NaBaYb}(\text{BO}_3)_2$, *Phys. Rev. Mater.* **3**, 094404 (2019).
- [36] S. Guo, R. Zhong, K. Górnicka, T. Klimczuk, and R. J. Cava, Crystal growth, structure, and magnetism of the 2D spin 1/2 triangular lattice material $\text{Rb}_3\text{Yb}(\text{PO}_4)_2$, *Chem. Mater.* **32**, 10670 (2020).
- [37] H. D. Zhou, C. Xu, A. M. Hallas, H. J. Silverstein, C. R. Wiebe, I. Umegaki, J. Q. Yan, T. P. Murphy, J. H. Park, Y. Qiu, J. R. D. Copley, J. S. Gardner, and Y. Takano, Successive Phase Transitions and Extended Spin-Excitation Continuum in the $S = 1/2$ Triangular-Lattice Antiferromagnet $\text{Ba}_3\text{CoSb}_2\text{O}_9$, *Phys. Rev. Lett.* **109**, 267206 (2012).
- [38] K. Yokota, N. Kurita, and H. Tanaka, Magnetic phase diagram of the $S = 1/2$ triangular-lattice Heisenberg antiferromagnet $\text{Ba}_3\text{CoNb}_2\text{O}_9$, *Phys. Rev. B* **90**, 014403 (2014).
- [39] J. Iaconis, C. Liu, G. B. Halasz, and L. Balents, Spin Liquid versus Spin Orbit Coupling on the Triangular Lattice, *SciPost Phys.* **4**, 003 (2018)
- [40] J. Rodriguez-Carvajal, Recent advances in magnetic structure determination by neutron powder diffraction," *Physica B: Condens. Matter* **192**, 55 (1993).
- [41] P. Hohenberg and W. Kohn, Inhomogeneous Electron Gas, *Phys. Rev.* **136**, B864 (1964).
- [42] R. O. Jones and O. Gunnarsson, The density functional formalism, its applications and prospects, *Rev. Mod. Phys.* **61**, 689 (1989).
- [43] A. I. Liechtenstein, V. I. Anisimov, and J. Zaanen, Density-functional theory and strong interactions: Orbital ordering in Mott-Hubbard insulators, *Phys. Rev. B* **52**, R5467 (1995).
- [44] K. Schwarz and P. Blaha, Solid state calculations using WIEN2k, *Computational Materials Science* **28**, 259 (2003).
- [45] J. Kunes, R. Arita, P. Wissgott, A. Toschi, H. Ikeda, and K. Held, Wien2wannier: From linearized augmented plane waves to maximally localized Wannier functions, *Computer Physics Communications* **181**,1888 (2010).
- [46] A. A. Mostofi, J. R. Yates, Y.-S. Lee, I. Souza, D. Van-

- derbilt, and N. Marzari, An updated version of wannier90: A Tool for Obtaining Maximally-Localised Wannier Functions, *Computer Physics Communications* **178**, 685 (2008).
- [47] O. K. Andersen, Linear methods in band theory, *Phys. Rev. B* **12**, 3060 (1975).
- [48] J. M. Wills and B. R. Cooper, Synthesis of band and model Hamiltonian theory for hybridizing cerium systems, *Phys. Rev. B* **36**, 3809 (1987).
- [49] J. M. Wills, O. Eriksson, M. Alouini, and D. L. Price, *Electronic Structure and Physical Properties of Solids: The Uses of the LMTO Method* (Springer-Verlag, Berlin, 2000).
- [50] A. I. Liechtenstein, M. I. Katsnelson, V. P. Antropov, and V. A. Gubanov, Local spin density functional approach to the theory of exchange interactions in ferromagnetic metals and alloys, *J. Mag. Mag. Mat.* **67**, 65 (1987).
- [51] M. I. Katsnelson and A. I. Liechtenstein, First-principles calculations of magnetic interactions in correlated systems, *Phys. Rev. B* **61**, 8906 (2000).
- [52] Y. O. Kvashnin, O. Grånäs, I. Di Marco, M. I. Katsnelson, A. I. Liechtenstein, and O. Eriksson, Exchange parameters of strongly correlated materials: Extraction from spin-polarized density functional theory plus dynamical mean-field theory, *Phys. Rev. B* **91**, 125133 (2015).
- [53] A. Grechnev, I. Di Marco, M. I. Katsnelson, A. I. Liechtenstein, J. Wills, and O. Eriksson, Theory of bulk and surface quasiparticle spectra for Fe, Co, and Ni, *Phys. Rev. B* **76**, 035107 (2007).
- [54] I. Di Marco, J. Minár, S. Chadov, M. I. Katsnelson, H. Ebert, and A. I. Liechtenstein, Correlation effects in the total energy, the bulk modulus, and the lattice constant of a transition metal: Combined local-density approximation and dynamical mean-field theory applied to Ni and Mn, *Phys. Rev. B* **79**, 115111 (2009).
- [55] P. Thunström, I. Di Marco, A. Grechnev, S. Lebègue, M. I. Katsnelson, A. Svane, and O. Eriksson, Multiplet effects in the electronic structure of intermediate-valence compounds, *Phys. Rev. B* **79**, 165104 (2009).
- [56] O. Grånäs, I. Di Marco, P. Thunström, L. Nordström, O. Eriksson, T. Björkman, and J. Wills, Charge self-consistent dynamical mean-field theory based on the full-potential linear muffin-tin orbital method: Methodology and applications, *Computational Materials Science* **55**, 295 (2012).
- [57] F. Aryasetiawan, M. Imada, A. Georges, G. Kotliar, S. Biermann, and A. I. Liechtenstein, Frequency-dependent local interactions and low-energy effective models from electronic structure calculations, *Phys. Rev. B* **70**, 195104 (2004).
- [58] L. Vaugier, H. Jiang, and S. Biermann, Hubbard U and Hund exchange J in transition metal oxides: Screening versus localization trends from constrained random phase approximation, *Phys. Rev. B* **86**, 165105 (2012).
- [59] P. W. Selwood, *Magnetochemistry* (Wiley-Interscience, New York, 1956) 2nd ed., Chapter 2, page 78.
- [60] K. I. Kugel and D. I. Khomskii, Crystal structure and magnetic properties of substances with orbital degeneracy, *Sov. Phys.-JETP* **37**, 725 (1973).